



Depth-profile of impairments in endothelin-I – induced focal cortical ischemia

Daria Vinokurova^{1,2,*}, Andrey Zakharov^{1,3,*} ,
 Kseniya Chernova¹, Gulshat Burkhanova-Zakirova¹,
 Viktor Horst⁴ , Coline L Lemale⁴, Jens P Dreier^{4,5,6}  and
 Roustem Khazipov^{1,2} 

Abstract

The development of ischemic lesions has primarily been studied in horizontal cortical space. However, how ischemic lesions develop through the cortical depth remains largely unknown. We explored this question using direct current coupled recordings at different cortical depths using linear arrays of iridium electrodes in the focal epipial endothelin-I (ETI) ischemia model in the rat barrel cortex. ETI-induced impairments were characterized by a vertical gradient with (i) rapid suppression of the spontaneous activity in the superficial cortical layers at the onset of ischemia, (ii) compartmentalization of spreading depolarizations (SDs) to the deep layers during progression of ischemia, and (iii) deeper suppression of activity and larger histological lesion size in superficial cortical layers. The level of impairments correlated strongly with the rate of spontaneous activity suppression, the rate of SD onset after ETI application, and the amplitude of giant negative ultraslow potentials (~ -70 mV), which developed during ETI application and were similar to the tent-shaped ultraslow potentials observed during focal ischemia in the human cortex. Thus, in the epipial ETI ischemia model, ischemic lesions develop progressively from the surface to the cortical depth, and early changes in electrical activity at the onset of ETI-induced ischemia reliably predict the severity of ischemic damage.

Keywords

DC-recordings, endothelin, ischemia, somatosensory cortex, spreading depolarization

Received 7 January 2022; Revised 29 April 2022; Accepted 21 May 2022

Introduction

Most knowledge about the development of ischemic cortical lesions is based primarily on explorations in the horizontal cortical plane. Yet the cerebral cortex is a three-dimensional structure composed of up to six layers, as in the somatosensory cortex, where the generation of spontaneous and somatosensory-induced network activities involves dynamic interactions between thalamocortical inputs and intracortical circuits within and between cortical layers.¹ How ischemic lesions develop in the vertical dimension through the layers of the cerebral cortex, however, remains largely unknown. This question is also of great clinical importance, because the interpretation of electrical signals at the brain surface during conventional scalp EEG or electrocorticography (ECoG) recordings in patients

¹Laboratory of Neurobiology, Kazan Federal University, Kazan, Russia

²INMED, Aix-Marseille University, Marseille, France

³Department of Physiology, Kazan State Medical University, Kazan, Russia

⁴Centre for Stroke Research Berlin, Department of Experimental Neurology and Department of Neurology, Charité Universitätsmedizin Berlin (Corporate Member of Freie Universität Berlin, Humboldt-Universität zu Berlin, and Berlin Institute of Health), Berlin, Germany

⁵Bernstein Centre for Computational Neuroscience Berlin, Berlin, Germany

⁶Einstein Centre for Neurosciences Berlin, Berlin, Germany

*These authors contributed equally to this work.

Corresponding author:

Roustem Khazipov, INMED/INSERM U1249, 134 avenue de Luminy BPI3, 13273 Marseille, France.

Email: roustem.khazipov@inserm.fr

requires knowledge of their generation mechanisms within the cortex.² This is true not only for physiological activity patterns, which typically display depression during ischemia, but also for pathological patterns of spreading depolarizations (SDs) and SD-initiated negative ultraslow potentials (NUPs) emerging during ischemia and serving as reliable markers of ischemic injury.^{3–6} NUPs are of special interest as this pattern has not been previously reported in animal models of cortical ischemia. Despite the high diagnostic value of NUPs for prediction of ischemic injury, they remain poorly understood and may involve not only biological potentials generated by the injured cortex but also the sensitivity of noble metal electrodes to oxygen and different ions.⁷

To investigate these questions, in the present work, we used the brain-topical endothelin-1 (ET1) model and linear multichannel silicone probes with iridium electrodes implanted vertically in the cortex. ET1 is a potent cerebrovascular constrictor.⁸ Application of ET1 at concentrations of 100 nM or greater to the adventitial surface of the exposed middle cerebral artery results in transient ischemia and infarction in the middle cerebral artery territory.⁹ Epipial ET1 application in ascending concentrations of 10 nM and above results in gradually developing ischemia leading to selective neuronal damage in the hypoperfused area when either at least one SD developed in the hypoperfused area or an SD was artificially triggered outside the hypoperfused area and invaded the hypoperfused area.^{10,11} In contrast, epipial application of ET1 at a concentration of 1 μ M results in cortical infarction, the size of which depended primarily on the area of the exposed cortex.

The ET1 model of transient focal ischemia has provided important insights into electrophysiological changes during ischemia, including persistent depression of physiological activity at the ischemic focus and distant areas with eventual recovery only in distant areas, and demonstration of the instrumental roles of SDs in ET1-induced neuronal death.^{12,13} The ET1 model allows SDs and changes in electrical activity during ischemia and reperfusion to be correlated with lesion size. In this regard, early electrographic changes in cortical activity during ischemia are of particular interest because they can serve as predictors of the onset of ischemic stroke and its severity, and may also be used as an alarm to initiate treatment during ongoing electrophysiological monitoring in patients at risk for ischemic complications.^{6,14–18}

In the present study, we explored alterations in electrical activity across layers of a cortical barrel column during transient (1 hour) focal ischemia produced by topical epipial ET1 application, followed by 3 hours of ET1 washout. Functional impairments were then

compared with histological lesion size, and retrospective analysis was used to estimate the predictive value of early neurophysiological changes at the onset of ischemia for predicting the severity of ischemic impairments.

Materials and methods

Ethical approval

The animal experiments were carried out in compliance with the ARRIVE guidelines. Animal care and procedures were in accordance with EU Directive 2010/63/EU for animal experiments, and all animal-use protocols were approved by the French National Institute of Health and Medical Research (APAFIS #16992-2020070612319346 v2) and the Local Ethical Committee of Kazan Federal University (№24/22.09.2020).

Animal preparation

Wistar rats of both sexes aged from 3 to 7 weeks were used. Animals were prepared under isoflurane anesthesia at the surgical level (4% for induction, 2% for maintenance, Fluotec4 (Surgivet/Anesco)), confirmed by a negative toe-pinch reflex. The skin above the skull and periosteum were removed, Hemostab (Omegadent, Moscow, Russia) was used to stop capillary bleeding and then was rinsed with 0.9% NaCl. The wound was treated with bupivacaine (0.25%). A metal ring was attached to the skull with dental cement (Grip Cement, Caulk Dentsply, DE, USA). Then isoflurane anesthesia was discontinued and the animals were administered urethane at the surgical level of anesthesia (1.5 g/kg, i.p.), confirmed by immobility, and the absence of vocalizations and negative toe-pinch reflexes during the entire experiment. During recordings, rats were placed on a heated platform (37 °C, TC-344B; Warner Instruments, Hamden, CT). The metal ring was attached to a magnetic stand via a ball-joint to restrain head movements. Chloride-coated silver wire was placed in the cerebellum to serve as a ground/reference electrode. A cranial window 3–4 mm in diameter was drilled above the barrel cortex area (~2.0 mm caudal and ~5.5 mm lateral from bregma) and a 1–2 mm high wall was made from dental cement around the cranial window to form the drug application chamber. To avoid drying of the cortical surface the chamber was regularly supplied with warm artificial cerebrospinal fluid (ACSF) of the following composition: 126 mM NaCl, 3.5 mM KCl, 1.2 mM NaH₂PO₄, 25 mM NaHCO₃, 20 mM glucose, 2 mM CaCl₂, 1.3 mM MgCl₂. The dura mater was cut in the area of electrode insertion in the vicinity of the distal

MCA branch to enable drug access to the pia mater. The ET1 (Sigma-Aldrich, USA) solution was prepared from 40 mM ET1 frozen PBS-stock solution to a final concentration of 0.1–2 μ M dissolved in ACSF on the day of the experiment. Prior to ET1 application, ACSF was removed from the application chamber using a KimTech wipe (USA) and ET1 was regularly applied at 10–15 min intervals for 1 hour. Then ET1 was removed from the chamber, the chamber was rinsed 3 times, and supplied with ACSF for 3 hours. In a separate set of animals, SD was induced by application of 1 M KCl to the epidural chamber. The high-potassium solution was rinsed with ACSF immediately after SD, and repetitive 1 M KCl applications were performed at 15 min intervals.

Electrophysiology

Recordings of the field potential (FP) and multiple unit activity (MUA) were performed using linear multi-channel silicone probes with iridium electrodes: 413 μ m² surface area, 100 μ m separation distance (A1x16-5-100-413-A16, Neuronexus Technologies, USA). The probe was inserted vertically into the barrel cortex to a depth of 1.6–1.8 mm. The probe was coated with DiI fluorescent dye (DiI, Sigma Aldrich, USA) for post-hoc reconstruction of the electrode position. The signals were amplified, lowpass filtered at 9 kHz and digitized at 32 kHz using a DigitalLynx (Neuralynx, USA) amplifier. Recordings were performed: (i) in true DC mode (input range \pm 131 mV) with DC potential offsets compensated at the onset of recordings as described previously¹⁹ or (ii) using full-band recordings with inverse filtering for signal reconstruction based on hybrid AC/DC-divider RRC filters.²⁰ The whiskers were trimmed to a length of 0.8–1.5 mm. A needle (22 G) was glued to the end of a piezo actuator and the tip of the whisker was inserted into the blunt tip of the needle. Single whiskers were deflected using a piezoelectric bending actuator (PAB-4010, Nihon Ceratec, Japan) using 200 ms square pulses at 5 s intervals. The principal whisker (PW) was identified by the shortest latency MUA responses in layer 4 and L5/6 border (Lb5/6) as described previously.²¹

Data analysis

Experimental data were processed using MATLAB environment (MathWorks, USA). Raw signals, FP and extracellular spikes were primarily processed using programs including ExpressAnalysis and Eview (AZ, <https://github.com/AndreyZakharovExp>). For FP analysis, the wide-band signal was downsampled to 1000 Hz using the *resample* function. Positive

polarity is shown as up in all figures except for Figure 7 where negative polarity is shown as up. For action potential detection, the raw wide-band signal was filtered (bandpass 300–5000 Hz) and negative deflections exceeding 5 standard deviations (STD) calculated over the most silent 1 s length segment of the filtered trace were considered as spikes. MUA during sensory evoked responses was counted within 0–30 ms after a stimulus and divided into early MUA (in a 6.2 ± 0.5 ms time window starting from 5.5 ± 0.2 ms after stimulus) and late MUA (in a 16 ± 1 ms time window starting 1.5 ± 0.2 ms after the end of the early evoked MUA); $n = 26$. Division of MUA into early and late was based on the MUA-density local minimum between these fractions.²¹ Sensory-evoked potential (SEP) amplitude was calculated as the first negative extremum after evoked potential onset at each channel. SEP slope was calculated as the minimum of the first derivative of the rising front of SEP. The UP-states of delta oscillations and troughs of spindles were detected as >3 STD FP deflections from L6 and L4, respectively. Current source density (CSD) was computed according to a differential scheme for the second spatial derivative of FP along the probe axis. Spectral FP analysis was performed using Chronux toolbox (<http://chronux.org>). Spectral power was estimated using a multi-taper estimator with padding factor two, five tapers and a time-bandwidth product corresponding to frequency bands and FP segment duration. We used the 0.5–2 Hz band for delta, 3–8 Hz for theta, 8–13 Hz for alpha, 13–30 Hz for beta, and 30–80 Hz for gamma frequency bands.

Histology

At the end of recordings, animals were deeply anaesthetized with urethane (3 g/kg, intraperitoneally) and perfused through the left cardiac ventricle with 4% paraformaldehyde +1% glutaraldehyde solution. The brains were removed and left for fixation at room temperature overnight. Then the brains were rinsed in PBS and cut in the coronal plane into 100 μ m-thick slices using a vibratome (Leica Biosystems, Wetzlar, Germany). Photographs were acquired using a light microscope (Olympus, Japan) in a white field. The morphometric ischemic lesion assessment was performed using ImageJ software (NIH, USA). Ischemic foci were digitally contrasted for manual definition of lesion borders. The size of ischemic focus was assessed in photographs with the DiI electrode traces. The length of lesion was measured in each layer taking into account cortical curvature.

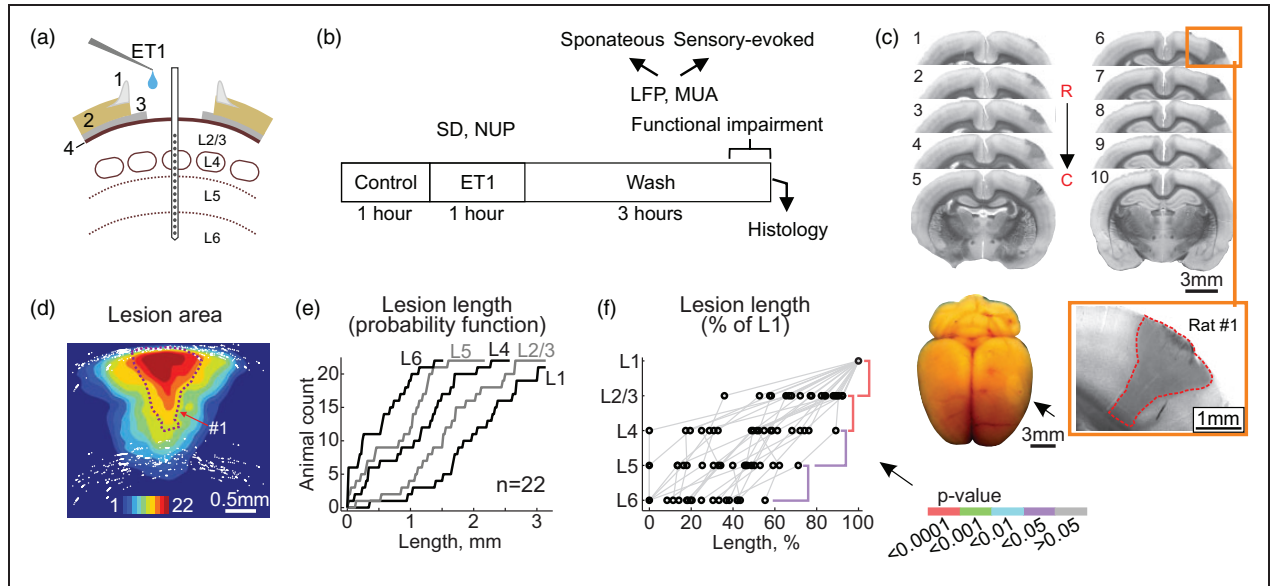


Figure 1. The ET1-induced ischemic focus is largest in the superficial cortical layers. (a) Experimental setup. ET1 is applied epidurally via a cranial window over the barrel cortex. A 16-channel linear Ir electrode array is inserted vertically in the center of the cranial window to record electrical activity from all layers of the cortical barrel column. 1, cement wall; 2, skull; 3, dura mater; 4, pia mater. (b) Experimental protocol. Recordings of spontaneous activity and principal whisker – evoked responses (field potentials, FP) and multiple unit activity (MUA) were performed for a 1-hour control period followed by 1-hour of ET1 application and 3-hours of ET1 washout. SD, spreading depolarization; NUP, negative ultraslow potential. After the recordings, the ischemic lesion was examined in coronal brain slices. (c) An example of consecutive coronal brain slices (0.1 mm thick, 1–10) in the rostral (R) to caudal (C) direction from rat #1. Slice 6 (outlined by a yellow box) with the trace of the electrode array is shown below at higher magnification. Note the conical shape of the ischemic focus, the borders of which are marked by a dashed red line, with a larger lesion in the superficial layers. Bottom left, an example of ischemic focus in the barrel cortex (pale oval area indicated by arrow) in an unsectioned brain. (d) Cumulative probability image of the ischemic lesion formed after 1 hour of ET1 exposure and 3 hours of ET1 washout, obtained by superimposing the lesion areas. White dots indicate cortical boundaries. (e) Probability function of lesion length in cortical layers and (f) Lesion length in cortical layers normalized to L1. p-values for cross-layer comparisons are color-coded according to the p-value scale bar. d–f: pooled data from 22 rats.

Statistical analysis

Statistical analysis was performed using the MATLAB Statistics toolbox. Pooled data are presented as median, 25th (Q1) and 75th (Q3) percentiles in box-plots or shaded areas. Kruskal-Wallis test was performed to assess the significance of differences between samples. Correlations were calculated as Spearman’s correlation coefficient with exact p-value. The level of significance was kept at $p < 0.05$.

Results

We explored the effects of ET1 on spontaneous and sensory-evoked activity across the layers of cortical barrel columns in urethane-anaesthetized, head-restrained rats during 1 hour of topical epidural application of ET1 and 3 hours of drug washout (Figure 1(a) and (b)). At the end of the recordings, the animals were sacrificed and the size of the ischemic lesion was measured in coronal sections. The morphological and functional alterations were compared in the ischemic focus

across cortical layers. The results will be presented in the following order: (i) we will describe the functional and morphological impairments across cortical layers in the ischemic focus formed after 1 hour of ET1 application and three hours of ET1 washout and (ii) we will characterize the changes in electrical activity during ET1 application focusing on the depth profiles of SDs and NUPs, and attempt to determine the electrophysiological events at the onset of ischemia that most accurately predict the severity of ischemic damage.

Morphometry of the ischemic focus. Histological examination of the ischemic focus formed after one hour of topical epidural ET1 (0.1–2 μM) application followed by three hours of ET1 washout was performed in 22 rats. On the surface of the extracted brains, ischemic lesions appeared as a round, pale area corresponding to the shape of the cranial window where ET1 was applied (Figure 1(c), bottom). Bright-field microscopy of coronal brain sections revealed a focal area of reduced light transmission in the region of ET1 application (Figure 1(c)). Morphological damage was limited to

the neocortex and no ischemic damage was observed in subcortical areas. Sections with DiI traces from the silicone probes (which were inserted in the center of the ET1-exposed area) typically had the largest lesion size and were used for morphometry of ischemic foci. The area of ischemic foci on these sections was 2.17 [0.90, 2.53] mm² (median [interquartile range]), range 0.16 to 4.7 mm² (n=22) which highly correlated with the lesion volume calculated from serial coronal sections (1.90 [0.94, 2.91] mm³, R=0.629, p<0.05, n=14). Lesions were generally conical in shape with a broad base at the cortical surface and a tip oriented toward cortical depth, and the length of the ischemic focus decreased from the cortical surface toward the depth (Figure 1(c) and (d)). Layer-specific assessment of focus size relative to layer 1 (L1), where lesion length was maximal, revealed a vertical gradient with a progressive reduction of horizontal lesion length from surface to depth (Figure 1(e) and (f)).

We next verified whether the vertical pattern of the structural lesion is specific for the site of ET1 application by injecting ET1 into the deep layers. Ischemic foci that formed after intracortical injection of ET1 (1 μM, 1–3 μl) at the depth of layers 5/6 (~1100 μm) differed significantly from those formed after epipial ET1 application (Supplementary Figure 1). In three cases (3/11), the spherical-shape focus around the ET1 injection site was limited to the deep layers. In the remaining cases (8/11), pillar-shaped lesions extended from the vertex to the white matter. On average, the vertical damage gradient characteristic of epipial ET1 application was not observed after intracortical ET1 injection. Taken together, these data suggest that the vertical lesion gradient observed during epipial ET1 administration is due to the vertical ET1 concentration gradient formed during ET1 diffusion from the surface into the cortex.

Depth profile of functional impairments in the ischemic focus.

We further assessed the depth profile of functional impairments in the ischemic focus by comparing the levels of suppression of spontaneous activity and sensory-evoked responses relative to control values during the third hour of ET1 washout. The analysis included a variety of FP and MUA characteristics, including spontaneous MUA and FP power in different frequency bands, as well as slope, amplitude, and peak delay of SEPs, and the elevation of MUA during the early and late phases of sensory responses evoked by principal whisker stimulation (Figure 2). All parameters showed suppression in the ischemic focus compared with control (pre-ET1) values in all layers. However, activity was more suppressed in the superficial layers than in the deep layers. Thus, spontaneous MUA after ischemia was suppressed to 0.4 [0.0, 40.3]%

(p<0.0001) and to 5.5 [0.3, 95.1]% (p<0.0001) of control values in L2/3 and L6, respectively, with intermediate suppression levels in L4 and 5 (Figure 2(a), (b) and (d)). MUA levels in the ischemic focus were also positively correlated with cortical depth (R=0.36; n=26; p<0.0001; Figure 2(b) and (c)). Similarly, the amplitude of SEPs in the ischemic focus reached 29 [16, 66]% (p<0.0001) and 74 [45, 96]% (p<0.0001) of control values in L2/3 and L6, respectively, and was positively correlated with cortical depth (R=0.51; n=26, p<0.0001) (Figure 2(c) and (d)). A vertical gradient with stronger suppression at the cortical surface was also characteristic of FP power in the theta, beta and gamma ranges, SEP slope and early MUA during sensory-evoked responses (Figure 2(c) and (d)), and sinks of SEPs, delta oscillations and spindle oscillations (Figure 2(d) and (e)). A few parameters, such as MUA during the late phase of the sensory response showed similar levels of suppression at all cortical depths (Figure 2(c) and (d)). Among all parameters, only delta power was less suppressed at the cortical surface than at the cortical depth (R=-0.33, p<0.0001), which was associated with more prominent suppression, or even conversion to source, of the UP-states' L2/3 sink (Figure 2(d) and (e)). The only parameter that did not change in the ischemic focus was the SEP delay (R=0.06, p>0.05) indicating that there was no change in signal conduction velocity from whiskers to cortex. Together with the histological findings, these results indicate that morphological and functional damage during ET1-induced focal ischemia develops from the cortical surface to the depth and that the superficial layers appear to be more affected than the deep layers.

Variability of ischemic damage. The size of the ischemic lesion and the level of functional impairment that developed after ET1 application varied considerably between animals. Therefore, in the next step, we explored the relationships between functional impairment and ischemic lesion size. Among the different parameters, the average spontaneous MUA in all layers (MUA*, measured at the end of the third hour of ET1 washout and normalized to control values) was chosen as the reference measure of functional impairment. The MUA* displayed large variability from 0 to 161% and reached, at the group level, 7.0 [0.6, 68.1]% (n=26). We found that the MUA* distribution could be fitted with a biexponential function ($\tau_1=1.1$ and $\tau_2=84$ Figure 3(a)). The median value of MUA* (7%) at the breakpoint of these two exponents was arbitrarily chosen to separate the "high" and "low" MUA* recovery groups (HR, 68.1 [24.7, 101.9]% (n=13) and LR, 0.6 [0.0, 1.8]% (n=13)). Histological lesion size was larger and extended

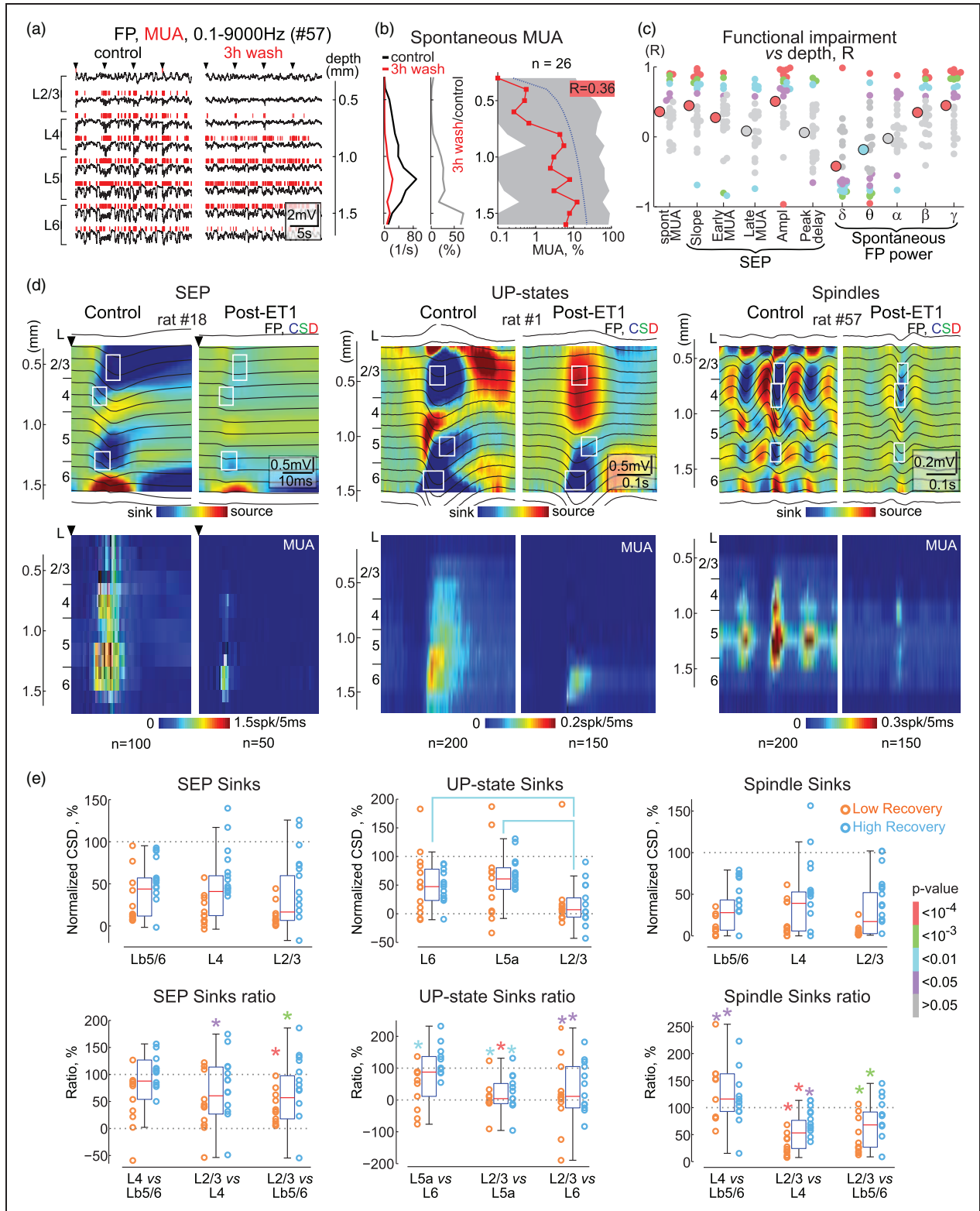


Figure 2. Vertical gradient of functional impairments in the ischemic focus. (a) Example of recordings of spontaneous activity in different cortical layers (FP, black traces and MUA, red vertical bars above) under control conditions (left) and at the end of the third hour of ET1 washout (right) in rat #57. Arrowheads indicate principal whisker deflections. (b) Corresponding MUA frequency across cortical depth in control conditions and in the ischemic focus (left, absolute values and middle, normalized to control) in rat #57. Right, depth profile of MUA frequency in the ischemic focus normalized to control values (n = 26). Red squares show median, shaded Continued.

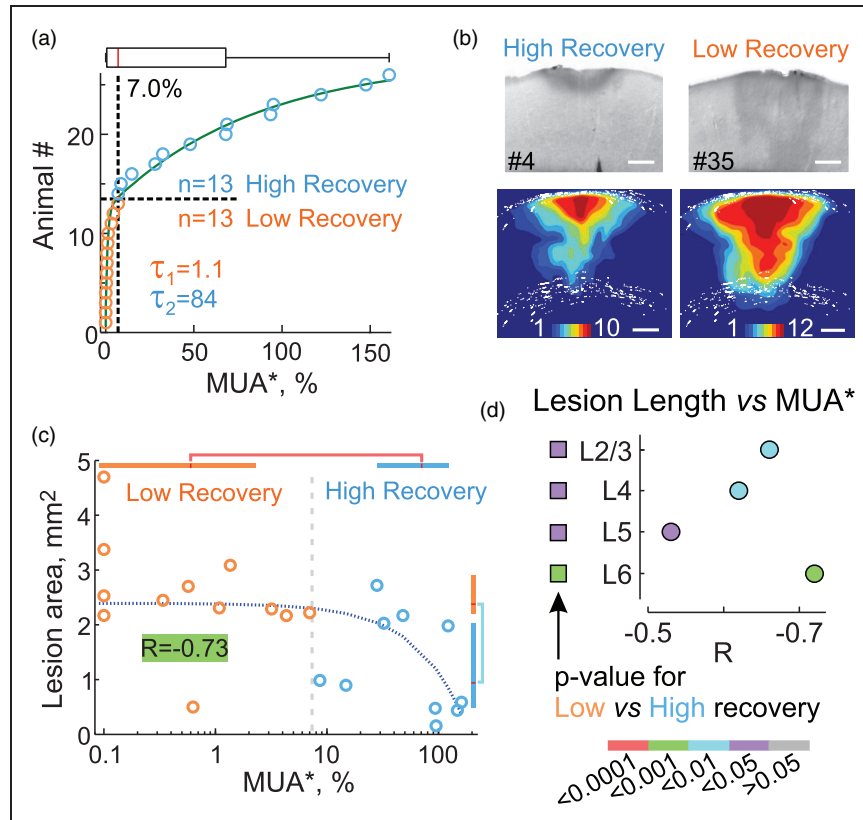


Figure 3. Variability of functional and morphological impairments in the ETI model. (a) Distribution of spontaneous MUA in the ischemic focus averaged over all layers (MUA*) in 26 rats. The breakpoint of the two-exponential fit (green line) at the value of 7% was used to separate animals into groups with either high (>7%, $n = 13$) or low (<7%, $n = 13$) MUA* recovery. This value also corresponds to the median of the MUA* distribution (red line in the box plot above). (b) Examples of ischemic lesions in animals in the high and low recovery groups. Bottom, cumulative probability maps of the ischemic focus in the high ($n = 10$) and low ($n = 12$) recovery groups. Scale bar, 0.5 mm. (c) Correlation analysis between ischemic lesion area and MUA* in the ischemic focus ($n = 22$). Color-coded box plots show Q1-Q3 intervals, red lines show median, p-values for comparisons are color-coded according to the scale bar in panel d, bottom. The blue dashed line shows the linear approximation fit, the background color of the correlation coefficient R indicates the p-value. (d) Layer-specific analysis of the correlation between ischemic lesion length and MUA* in the focus. Circles indicate R and p-values for each layer. Squares indicate p-values for the difference between the high and low recovery groups. The bar for p-values is shown at the bottom.

deeper into the cortex in animals in the LR group (2.38 [2.20, 2.89] mm² ($n = 12$)) than in the HR group (0.94 [0.48, 2.03] mm² ($n = 10$); $p < 0.01$) (Figure 3(b)). The size of the ischemic focus also correlated with MUA* in

the entire population without division into LR and HR groups (lesion area: $R = -0.73$, $p < 0.001$, $n = 22$) (Figure 3(c)); lesion volume: $R = -0.59$, $p < 0.05$, $n = 14$). The linear size of the ischemic lesion was also

Figure 2. Continued.

area shows Q1-Q3 intervals, blue dotted line shows linear approximation, R box shows correlation coefficient, and its background codes for p-value according to the p-value bar at the right of panel E. (c) Correlation analysis between suppression level and cortical depth for various parameters of spontaneous and sensory-evoked FP and MUA. Each small circle indicates the R -values of an individual animal, large circles indicate the R -values of the population. The color of the circle indicates the p-value according to the p-value bar at the right of panel E. Pooled data from 26 rats. (d) Average SEP, delta (UP-states) and spindle oscillations (FP, top panels and MUA, bottom panels) in control and at the end of the 3rd hour of ETI washout across the cortical depth, overlaid on the color-coded CSD and MUA density maps, respectively. White rectangles indicate the regions for calculation of the main sinks. (e) Levels of suppression of the main sinks following ETI treatment relative to control values for SEPs, UP-states of delta oscillations and spindle troughs (top panels) and the corresponding relative changes of the main sinks in the post-ETI cortex (bottom panels). Each circle indicates values from an individual animal, circle color indicates high and low recovery of MUA*. Note that sinks in the superficial layers of post-ETI cortex are more severely suppressed than deep sinks. Colored brackets and * indicate significant differences and their color indicates the p-value according to the p-value bar on the right. Pooled data from 26 rats. Lb5/6 denotes border between L5 and L6.

strongly correlated with MUA* in all cortical layers (Figure 3(d)). Although, in the entire population, the size of the ischemic lesions correlated poorly with the age of the animals ($R = 0.27$, $p > 0.05$, $n = 22$), MUA* depended on age ($R = -0.57$, $p < 0.01$; $n = 26$), and the animals in the HR group were younger than those in the LR group (MUA*: $p < 0.001$; $n = 26$; lesion area: $p < 0.01$; $n = 22$), suggesting that age may be an aggravating factor.

Suppression of spontaneous FP power and the slope and amplitude of SEPs, and MUA during the early and late phases of the sensory-evoked responses also correlated strongly with MUA* and the histological size of the ischemic focus (Supplementary Figure 2). Thus, ischemic focus formed after ET1 application is variable in both histological lesion size and levels of functional impairment, with a strong correlation between size and functional impairment. We further hypothesized that this variability allows, through retrospective analysis, estimation of the predictive value of electrophysiological changes during the acute phase of ischemia for the severity of ischemic damage.

Non-spreading depression at the onset of ischemia. Epipial ET1 induced suppression of spontaneous and sensory-evoked activity (so-called non-spreading depression²²) was typically followed by clusters of SDs nested in NUPs (Figure 4; see also Figures 5 and 6). Non-spreading depression developed within minutes of ET1 application and was associated with a reduction in spontaneous MUA, a reduction of FP power in all frequency bands, a reduction of SEP slope and amplitude, and reduction of MUA during the early and late phases of the sensory-evoked responses (Figure 4). Non-spreading depression developed more rapidly in superficial cortical layers than in deep cortical layers (Figure 4(c) and (d)) and its rate reliably predicted the severity of cortical injury (Figure 4(e)). Indeed, the rate of non-spreading depression was strongly correlated with MUA* and the size of histological lesion in ischemic foci formed after ET1 application (Figure 4(e)). Consistent with these results, non-spreading depression at the start of ET1 application developed faster and was more robust in the LR group than in the HR group (Figure 4(e)).

Spreading depolarizations. SD clusters appeared after the non-spreading depression phase, 5.8 [4.5, 11.0] min after the start of ET1 application in 22 of 26 animals. Examples of recordings of five consecutive SDs at different cortical depths are shown in Figure 5(a). The first SDs were always initiated in the superficial layers or L4 at a depth of 400 [293–500] μm ($n = 22$) and propagated from the point of initiation upward and downward through the entire cortical column

and were associated with transient suppression of MUA in all layers (Figure 5(a) to (d)). The first SD reached an amplitude of -19 [-18 , -25] mV in L4 and lasted 40 [23, 64] s ($n = 22$). The starting point of each consecutive SD progressively moved deeper into the cortex to a depth of 1370 [1250, 1448] μm for the fifth SD ($p < 0.001$) (Figure 5(b), (c) and (d)). In parallel with the deepening of the initiation point, SDs became compartmentalized in the deep layers and failed to propagate to the superficial layers, in which MUA failed to recover between SD episodes (Figure 5(a) and (b)). This was evidenced by an unchanged amplitude of consecutive SDs in L6 (depth 1.5 mm), but a gradual decrease in the amplitude of SDs in L4 and L2/3 (depth 0.9 and 0.3 mm, respectively) (Figure 5(e)). Importantly, compartmentalized SDs in the deep layers were barely visible at the cortical surface, suggesting that they can be easily overlooked during subdural ECoG recordings. Compartmentalization of consecutive SDs into the deep layers could be due to the use-dependent SD feature. Therefore, we explored the depth profiles of SDs evoked by repetitive epipial application of 1 M KCl in a separate set of animals. In contrast to ET1-induced SDs, the depth initiation of five consecutive SDs in the KCl experiments remained at a depth of 300 [250, 500] μm ($n = 9$ rats, Figure 5(f), (g) and (h)), and all consecutive SDs propagated through the entire column, with only transient suppression of MUA during SDs in all layers.

We next asked whether SDs might have prognostic value for ischemic injury in our model. To this end, we analyzed the correlation between SDs and the level of injury reached three hours after ET1 removal, assessed by measures of MUA* and histological lesions in the ischemic focus. Examples of L4 SD recordings from three animals in the LR group and three animals in the HR group (Figure 5(i)) indicate that the shorter the time to the first SD, the more severe the cortical damage. This relationship was also prominent when the SD plots and corresponding lesion areas and MUA* in the ischemic focus were ranked by the first SD delays (Figure 5(j)), and was confirmed by the strong relationships between first SD onset and MUA* in the focus ($R = 0.86$, $p < 0.0001$, Figure 5(k)), and between first SD onset and lesion size ($R = -0.62$, $p < 0.01$, Figure 5(l)). Accordingly, in the HR group the first SD developed later than in the LR group: 670 [388, 1086] s vs 299 [245, 345] s, respectively ($p < 0.001$). For the number of SDs during the ET1-application period, however, there was no significant correlation with MUA* and lesion size in the ischemic focus. Yet, cases without SDs (4/26 animals) had minimal functional and morphological damage (Figure 5(k) and (l)). We also failed to find any consistent correlation between SD waveform and outcome, as SD

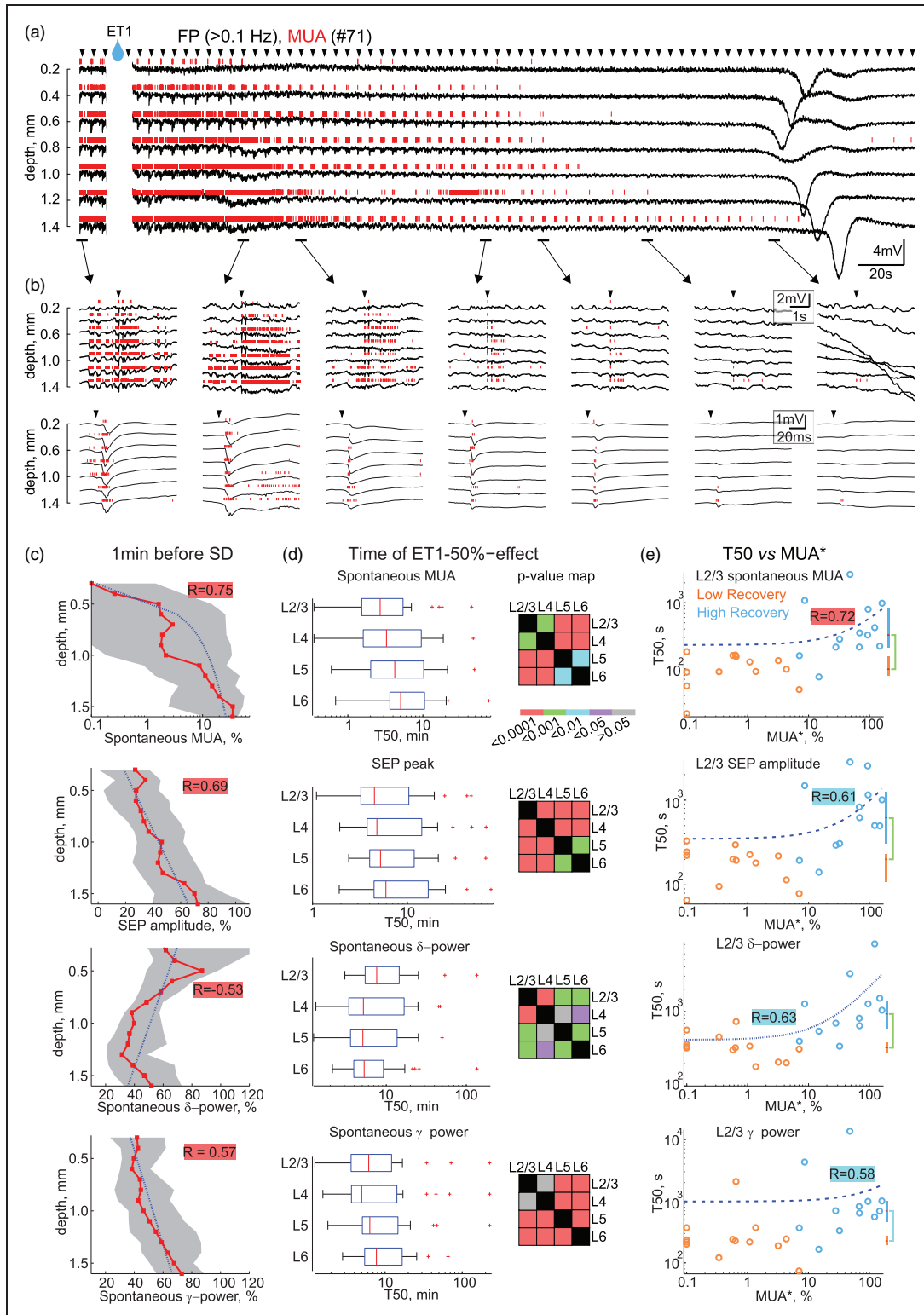


Figure 4. Depth-profile of non-spreading depression at the onset of ET1-evoked ischemia. (a) Example of recordings at different depths of a cortical barrel column at the beginning of ET1 application. Arrowheads above the traces indicate principal whisker deflections. Note the rapid suppression of spontaneous FP activity and MUA after ET1 application, which develops more rapidly in the superficial layers and precedes SD. (b) Parts of the recordings from panel a on an expanded time scale and examples of sensory-evoked responses. (c) Depth profile of suppression of spontaneous MUA frequency, SEP amplitude, delta and beta power 1 minute before SD. Layout as in Figure 2(b). (d) Half-time (T50) of suppression (left) and the corresponding p-value map for comparisons (right) of MUA frequency, SEP amplitude, delta and beta power in different layers. Box plots show Q1-Q3 borders, red lines show median values, whiskers show 5-95% intervals, red crosses are outliers. (e) Corresponding correlation analysis between T50 and MUA* in the ischemic focus for the same parameters measured in L2/3. Layout as in Figure 3(c).

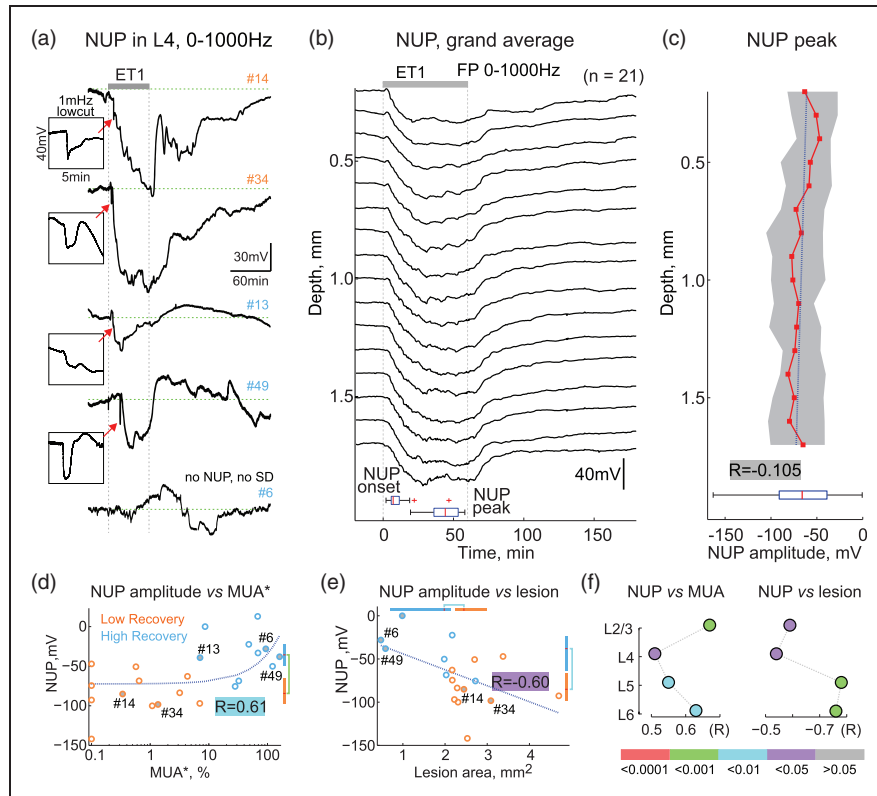


Figure 6. Negative ultraslow potentials and ischemic injury. (a) Examples of NUP (0-1000Hz) recorded from L4 during 1 hour of ET1 application and 3 hours of ET1 washout in two low recovery (orange #) and three high recovery (blue #) cases. Insets in the boxes show SDs at NUP onset on an expanded time scale. (b) Grand average depth profile of NUPs. Bottom, statistics on the onset and peak times of NUPs. (c) Depth profile of the NUP amplitude peak. Layout as in Figure 2(b). Bottom, distribution of NUP amplitude averaged over the entire cortical depth. (d and e) Correlation between NUP amplitude and MUA* in the ischemic focus (d) and ischemic lesion size (e). Layout as in Figure 3(c). (f) Correlation of NUP amplitude with MUA in the ischemic focus (left) and with ischemic lesion length (right) in different cortical layers. p-values are color-coded according to the bar below.

waveforms were severely hampered by the superposition of NUPs (see Figure 6(a)). Despite this, SDs represent a valuable marker in terms of delay of the first SD and SD expression for prediction of ischemic damage severity.

Negative ultraslow potentials. The first SDs heralded NUPs, which developed progressively through the duration of ET1 application, reaching an amplitude

of -68 [-87 , -40] mV ($n=22/26$, with SDs) and waned during ET1-washout (Figure 6(a) and (b)). NUPs involved all cortical layers (Figure 6(b)), and their amplitude did not depend on cortical depth ($R=-0.105$, $p=0.0584$; Figure 6(c)). We further assessed the correlations between NUPs and damage severity in the ischemic focus after ET1 washout. In agreement with clinical findings,⁴ the amplitude of NUPs was greater in cases with more severe ischemic

Figure 5. Continued.

(c) Depth profile of SD delays from the initiation point ($t=0$ ms). (d) Distribution of SD initiation point depths. (e) SD amplitudes normalized to the first SD at depths 0.3, 0.9 and 1.5 mm. (f) Depth profile of normalized SD amplitudes for five consecutive SDs during ET1 application. c-f: group data from 22 rats. (g) Distribution of SD initiation point depths for five consecutive SDs evoked by epipial IM KCl application (9 rats). (h) p-value map for comparisons of SD initiation depth in a series of consecutive SDs induced by ET1 ($n=22$) and IM KCl ($n=9$). (i) Examples of SD recordings from L4 during ET1 application in three cases with low recovery (orange #) and high recovery (blue #). Signals were high-pass filtered at >5 mHz to remove NUPs. (j) Left, overview of SDs (detected at any depth, vertical bars) during 1 hour of ET1 application ordered by the first SD delay from the start of ET1 application ($t=0$) in 26 rats. Middle, corresponding area of the ischemic lesion and MUA* in the ischemic focus. Right, corresponding amplitude of NUP. (k and l) Correlation between time to first SD from the start of ET1 application and MUA* in the ischemic focus (k) and ischemic lesion size (l). Layout as in Figure 3(c). (m) Mean number of SDs per animal (black line) and probability of SD occurrence (gray line) throughout ET1 application.

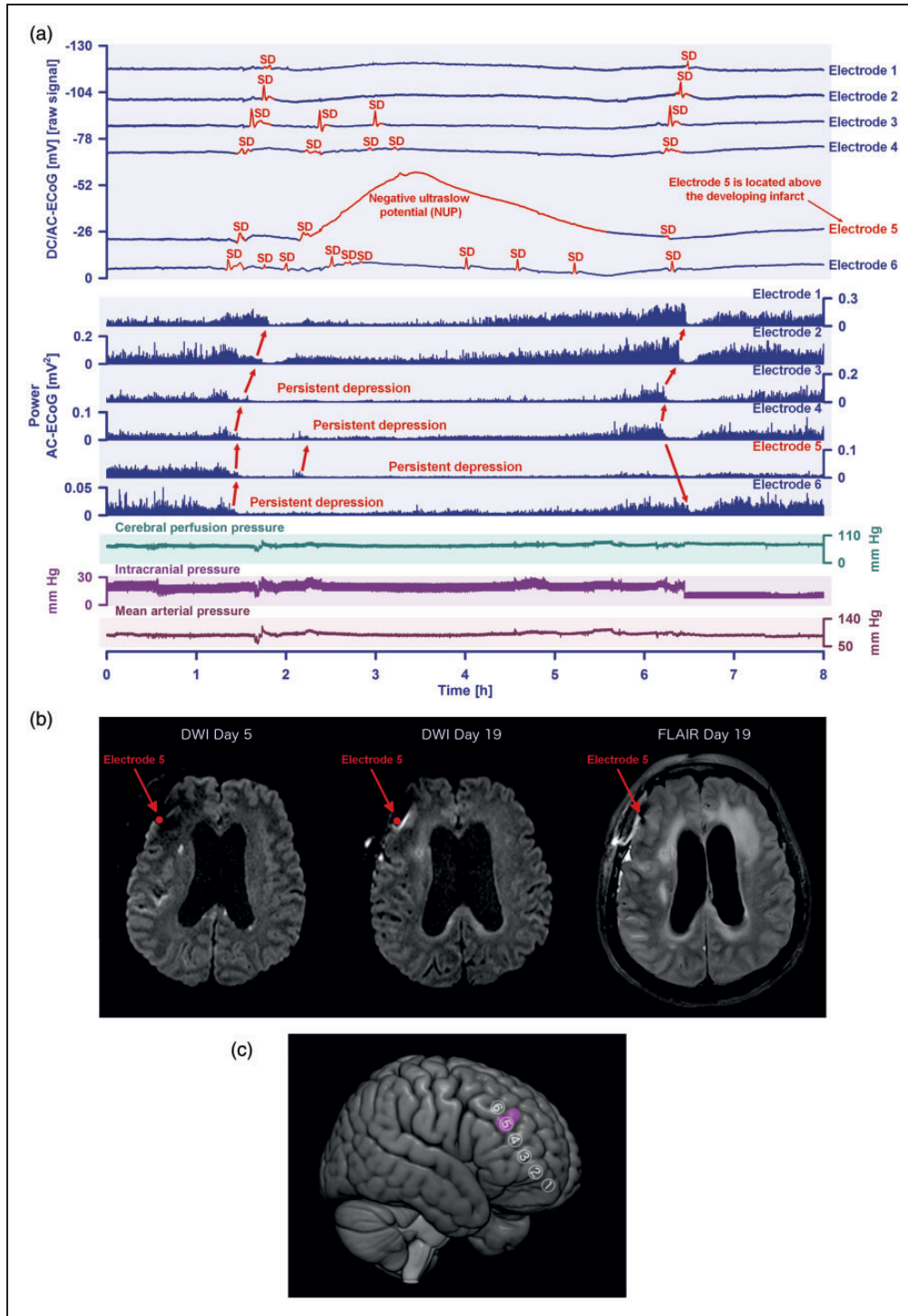


Figure 7. (a) This 64-year-old woman with aneurysmal subarachnoid hemorrhage (aSAH) showed a cluster of ten spreading depolarizations (SDs) that occurred during six hours on the seventh day after the initial hemorrhage. The patient was enrolled at Charité – Universitätsmedizin Berlin in the prospective, observational, multicenter, cohort, diagnostic phase III trial ‘DISCHARGE-1’.⁶ Traces 1 to 6 from top to bottom give the direct current (DC)/alternating current (AC)-electrocorticography (ECoG) recordings (bandpass: 0–45 Hz) at electrodes 1–6. SDs are observed as a negative DC shift (marked in red, negative voltage changes are shown as upward deflections following the EEG polarity convention). SDs propagated across the cortex from electrode 6 to 1. Selectively at electrode 5, the second SD resulted in a negative ultraslow potential (NUP) of high amplitude (–37.9 mV) lasting for ~3.8 hours. The following 6 traces (7 to 12) show the depressive effect of the SDs on the spontaneous brain activity as assessed in the higher
Continued.

damage. Thus, MUA* in the ischemic focus was strongly correlated with NUP amplitude ($R=0.61$, $p<0.01$; Figure 6(d)). Accordingly, NUPs in the HR group were smaller than in the LR group (-36 [-50 , -22] mV vs. -84 [-98 , -66] mV, respectively ($p<0.001$)). The correlation between NUP amplitude and MUA suppression was also significant in all cortical layers (Figure 6(f)). The amplitude of NUPs also correlated with the size of the ischemic lesion (Figure 6 (e); $R=-0.60$, $p=0.0105$), and with the length of the ischemic focus in all cortical layers (Figure 6(f), Supplementary Figure 3). Thus, NUPs are a robust feature of the acute phase of ischemia in the ET1-model, and their amplitude correlates with the level of ischemic injury.

Discussion

The main findings of the present study are twofold. First, we observed a vertical gradient of impairment with deeper suppression of activity and larger histological lesion size in superficial than deep cortical layers in ischemic foci formed after ET1 application. Second, we found that the levels of functional and morphological impairments in the ischemic foci are strongly correlated with specific electrophysiological changes at the onset of ischemia including the rate of onset of the first SD after ET1 application and the amplitude of NUPs. Of note, this study demonstrates for the first time giant-amplitude SD-initiated NUPs developing in an animal model of cortical ischemia and shows very good agreement with the observation of giant-amplitude NUPs in humans.

Ischemic foci formed in somatosensory cortex after transient ET1-evoked ischemia were conical in shape with a broad base at the cortical surface and a tip oriented toward cortical depth, and the horizontal length of the ischemic focus was several fold longer in superficial than deep layers. Morphologically, they resemble bell-shaped brain lesions secondary to aSAH due to ruptured aneurysms described in the autopsy

study by Stoltenburg-Didinger and Schwarz.²³ Supplementary Figure 4 provides an example of an MRI-proven early wedge-shaped infarct seen in an aSAH patient of the DISCHARGE-1 population (Dreier et al., 2022). Wedge-shaped infarcts with a triangular infarct rim with its base pointing toward the cortical surface were also reported in the primate clot model of cerebral ischemia after aSAH.²⁴ In this study, both horizontal and vertical infarcts were located exclusively in areas adjacent to subarachnoid blood, while the presence of a cortical infarct did not correlate with the degree of middle cerebral artery vasospasm. Our results are also consistent with the larger infarct size in the superficial cortical layers, which was evident, although not quantified in previous studies using the ET1 model in rodents (see Figure 3 of literature,⁹ Figures 3 and 4 of literature,²⁵ Figure 1 of literature,²⁶ and Figure 1 of literature²⁷ note that the latter paper also shows greater infarcts in the superficial layers in the MCAO model. In keeping with histological results, recordings of neuronal activity at different depth of the ischemic foci formed after ET1 application also revealed more severe functional impairments to the superficial than deep layers. Most of the functional parameters including FP power, sensory-evoked potentials and associated neuronal firing showed stronger depression in the superficial layers of the ischemic focus. Among all parameters, only delta power was less suppressed at the cortical surface than at the cortical depth which is consistent with the relative resistance of delta oscillations at the cortical surface compared to fast activities.^{15–18} Altogether, assessments of morphological and functional damage evoked by ET1-induced focal ischemia across cortical depth indicate that the superficial layers appear to be more affected than the deep layers. In keeping with these findings and the lack of a top-down lesion gradient following intracortical ET1 injections, we suggest that the preferential damage to the superficial layers during epileptic ET1 administration is due to the

Figure 7. Continued.

frequency band (AC-ECOG, bandpass: 0.5–45 Hz). Note that the activity depression propagated together with the SDs in the tissue (red arrows). The first SD caused a relatively short depression of spontaneous activity at electrodes 1 and 2, while it caused persistent depression of spontaneous activity at electrodes 3–6. Thus, SDs 2 to 10 partially propagated in electrically silent tissue and are classified accordingly as isoelectric-SDs (Dreier et al. 2017). Of note, the longest SD-induced activity depression is found at electrode 5 (trace 11) where the NUP occurred and the longitudinal MRIs showed the small delayed cortical infarct (cf. b). Trace 13 provides cerebral perfusion pressure (= mean arterial pressure – intracranial pressure). Trace 14 shows intracranial pressure measured via extraventricular drainage (EVD) catheter. Trace 15 shows mean arterial pressure (measured via radial artery catheter). (b) Comparison between the early postoperative MRI on day five and the late MRI on day 19 revealed a new hyperintensity anteromedial to electrode five on the late diffusion-weighted image (DWI) and an increased signal on the corresponding fluid-attenuation inversion recovery (FLAIR) image. This is consistent with a small delayed cortical infarct next to electrode 5 that developed between day five and 19. One has to look carefully to see this, not only because the lesion was relatively small, but also because of a signal loss anterosuperior to electrode 5 due to a titanium clamp used for bone flap fixation. (c) The 3D scheme illustrates ECoG electrodes 1 to 6 in relation to the delayed infarct (purple).

top-down gradient of ET1 concentration and the associated vasoconstriction/blood flow gradient during ET1 diffusion from the surface, and thus there is more severe ischemia in the superficial layers. In future experiments, it would be interesting to test this hypothesis using depth-resolved blood flow/perfusion assessment. Complete reconstruction of the dynamic changes in blood perfusion across the cortical depth should also consider the complex organization of anastomosed cortical microvasculature.²⁸

The acute functional changes in cortical activity during ET1 application were also in agreement with the vertical development of ischemic damage from the cortical surface to the depth. Indeed, the development of non-spreading depression showed a vertical pattern, with faster and deeper suppression of spontaneous MUA, FP power in the alpha and gamma (but not delta) bands and sensory-evoked responses at the superficial layers. Non-spreading depression is probably an adaptive mechanism activated to reduce metabolic demand and to maintain vital functions such as ionic gradients and membrane potential.^{29–31} It involves selective inhibition of glutamate release via presynaptic A1 adenosine receptors as a result of ATP degradation and elevated extracellular adenosine levels.^{32–36} Thus, it is plausible that gradual ischemia along the cortical depth is associated with a gradient in extracellular adenosine concentration, with higher adenosine levels and deeper suppression of activity in the superficial layers. The correlation between the rate of non-spreading depression of cortical activity at the onset of ischemia and the level of morphological and functional impairment in the ischemic focus can probably also be explained by more severe ischemia and more rapid elevation of adenosine levels at ischemia onset in cases with low recovery.

Our results support the critical role of SDs in the development of cortical injury during ischemia.^{3,22,37–39} There is ample evidence that SDs generated in metabolically deprived tissue deplete intracellular energy stores and, therefore, neurons fail to restore transmembrane ionic gradients and lose membrane potential.^{3,13,29,30,40–43} As a result, neurons die after a passage through the “commitment point”.^{37,42} Thus, the ischemic core expands, overcoming, by virtue of SDs, surrounding cortical territories.^{39,44–47} The present results suggest that this previously elaborated scenario for the development of ischemic damage in the horizontal cortical plane also works in the vertical cortical dimension. Indeed, we found that first SD delay from the start of ET1 application was strongly correlated with the severity of damage in the ischemic focus, likely reflecting the level of vasoconstriction and ischemia. Secondly, we found that the vertical organization of SDs undergoes significant changes during the

progression of ischemic injury. The first SDs in clusters were generated in the superficial or granular layers and propagated through the entire cortical column, which is consistent with the SD propagation pattern in the oxygen-glucose deprivation model of ischemia *in vitro*.^{48–51} However, the initiation point of subsequent SDs in clusters shifted downward with progression of ischemia, and SDs compartmentalized in deep layers. Ongoing activity recovered poorly during inter-SD periods in the superficial layers, similar to the persistent depression of ECoG activity between recurrent SDs indicative of tissue at risk.^{52–54} These observations are compatible with a progressive development of ischemic injury from the cortical surface to depth. Interestingly, the presence of SD indicates at least partial viability of the cortex at a given depth, while the absence of SD may be due to permanent depolarization manifested as a lack of MUA recovery, or alternatively, to low levels of ischemia manifested as persistence of MUA and spontaneous activity. This probably explains the lack of significant correlation between the number of SDs during ET1 application and the severity of damage in the ischemic focus as also noted in the MCAO model.⁴¹ It should be noted that SDs compartmentalized to deep layers were of smaller amplitude or absent at the cortical surface, which may also explain the variability in SD amplitude in ischemic SD clusters during ECoG recordings.^{13,41,55}

This study demonstrates for the first time giant-amplitude SD-initiated NUPs developing in an animal model of cortical ischemia. This shows very good agreement with the observation of giant-amplitude NUPs in humans. In humans, these occur in the cortex as an electrocorticographic correlate of infarction or brain death and can reach negative amplitudes with magnitudes greater than 100 mV.^{4,5,13,39,56–58} The SD-initiated NUP may even be detected in the context of relatively small cortical infarcts. In Figure 7, we show for the first time an illustration of the electrocorticographic generation of the smallest infarct to date in which the SD-initiated NUP has ever been measured in humans. A so-called delayed infarct is shown that developed in a patient with aneurysmal subarachnoid hemorrhage (aSAH) below electrode 5 between two MRIs on days 5 and 19. Neuromonitoring and longitudinal neuroimaging were performed in the patient as part of the.⁶ On day 7 after the initial hemorrhage, a cluster of 10 SDs developed. The first SD resulted in spreading depression of spontaneous activity at all electrodes. The depression of spontaneous activity persisted at electrodes 3–6 (interelectrode distance 1 cm) but recovered over several hours in electrodes 3, 4, and 6 in contrast to the spontaneous activity at electrode 5. The second SD exclusively initiated a giant-amplitude, tent-like NUP at electrode 5 as the typical electrocorticographic correlate

of infarct development in the human brain.⁴ During SD in hypoxic rats, this peculiar shape and high amplitude of the NUP could also be observed using brain surface platinum/iridium plate electrodes in contrast to intracortical Ag/AgCl-based glass microelectrodes.⁵⁸ Therefore, it was hypothesized that high amplitude and tent-like appearance of the NUP in humans at least partially result from the catalytic capacity for many chemical reactions that platinum/iridium electrodes have in biological media.⁴ In particular, unlike Ag/AgCl electrodes, they are oxygen and pH sensitive.⁷ The same is true for the iridium electrodes used here in rats (Supplementary Figure 5). The demonstration that similar giant-amplitude, tent-like NUPs measured with similar electrodes can also be measured in an animal ischemia model is important further evidence that these events detected in neuromonitoring in patients during neurocritical care are indeed indicative of infarct development and therefore represent a medical emergency. In this context, the etiology of ischemia (vasoconstriction, thrombotic or embolic vascular occlusion, or SD-induced spreading ischemia) probably does not play a crucial role in the potential generation of the NUP. Rather, we assume that SD-initiated NUP is a universal electrocorticographic hallmark of severe ischemia and hypoxia, which amplitude and shape when using platinum/iridium or iridium electrodes is not only dependent on the biological FP but also on chemical interferences at the electrode surface. The reasons why these electrodes in particular are used in humans have recently been explained in more detail by Major and colleagues.⁷

In conclusion, our study provides descriptions of the development of ischemic damage in the ET1 model in the vertical cortical dimension. We have shown that ischemic injury in the epipial ET1 model develops progressively from the cortical surface to the depth. This process is associated with compartmentalization of SDs in the deep layers, and the development of NUPs during the progression of ET1-induced ischemia. We also found that cortical impairments correlated with SD delay and with NUP amplitude. These results are important for understanding the development of cortical damage during focal ischemia in three-dimensional cortical space.

Funding

The author(s) disclosed receipt of the following financial support for the research, authorship, and/or publication of this article: This work was supported by RSF 22-15-00236 (electrophysiological experiments, histology and data analysis in rodents) and the subsidy No. 0671-2020-0059 allocated to Kazan Federal University for the state assignment in the sphere of scientific activities (development of the analytical software Eview) and performed in the framework of the Kazan Federal University Strategic Academic Leadership Program (PRIORITY-2030). JD received grants from the Deutsche

Forschungsgemeinschaft (DFG DR 323/5-1; DFG DR 323/10-1) and Bundesministerium fuer Bildung und Forschung (Era-Net Neuron EBio2, with funds from BMBF 01EW2004) (electrophysiological recordings and data analysis in patients).

Acknowledgements

The authors thank Drs. Valerie Crepel, Rosa Cossart for their valuable comments on the manuscript.





Declaration of conflicting interests

The author(s) declared no potential conflicts of interest with respect to the research, authorship, and/or publication of this article.

Authors' contributions

RK conceptualized the study. RK and JPD interpreted the findings and drafted the manuscript. DV, AZ, KC, GBZ performed the experiments. AZ, DV and RK analysed data. DV, AZ, KC, GBZ, VH, CLL revised the manuscript and interpreted the data. RK and AZ obtained funding for the project.

ORCID iDs

Andrey Zakharov  <https://orcid.org/0000-0002-6175-9796>
 Viktor Horst  <https://orcid.org/0000-0003-1282-881X>
 Jens P Dreier  <https://orcid.org/0000-0001-7459-2828>
 Roustem Khazipov  <https://orcid.org/0000-0002-6763-2841>

Supplemental material

Supplemental material for this article is available online.

References

1. Feldmeyer D, Brecht M, Helmchen F, et al. Barrel cortex function. *Prog Neurobiol* 2013; 103: 3–27.
2. Herreras O. Local field potentials: Myths and misunderstandings. *Front Neural Circuits* 2016; 10: 101.
3. Hartings JA, Shuttleworth CW, Kirov SA, et al. The continuum of spreading depolarizations in acute cortical lesion development: examining Leao's legacy. *J Cereb Blood Flow Metab* 2017; 37: 1571–1594.
4. Luckl J, Lemale CL, Kola V, et al. The negative ultraslow potential, electrophysiological correlate of infarction in the human cortex. *Brain* 2018; 141: 1734–1752.
5. Drenckhahn C, Winkler MK, Major S, et al. Correlates of spreading depolarization in human scalp electroencephalography. *Brain* 2012; 135: 853–868. Mar
6. Dreier JP, Winkler MKL, Major S, et al. Spreading depolarizations in ischaemia after subarachnoid haemorrhage, a diagnostic phase III study. *Brain* 2022; 145: 1264–1284.
7. Major S, Gajovic-Eichelmann N, Woitzik J, et al. Oxygen-induced and pH-induced direct current artifacts on invasive platinum/iridium electrodes for electrocorticography. *Neurocrit Care* 2021; 35: 146–159.

8. Yanagisawa M, Kurihara H, Kimura S, et al. A novel potent vasoconstrictor peptide produced by vascular endothelial cells. *Nature* 1988; 332: 411–415.
9. Macrae IM, Robinson MJ, Graham DI, et al. Endothelin-1-induced reductions in cerebral blood flow: dose dependency, time course, and neuropathological consequences. *J Cereb Blood Flow Metab* 1993; 13: 276–284.
10. Dreier JP, Kleeberg J, Petzold G, et al. Endothelin-1 potently induces Leao's cortical spreading depression in vivo in the rat: a model for an endothelial trigger of migrainous aura? *Brain* 2002; 125: 102–112.
11. Dreier JP, Kleeberg J, Alam M, et al. Endothelin-1-induced spreading depression in rats is associated with a microarea of selective neuronal necrosis. *Exp Biol Med (Maywood)* 2007; 232: 204–213.
12. Oliveira-Ferreira AI, Major S, Przesdzing I, et al. Spreading depolarizations in the rat endothelin-1 model of focal cerebellar ischemia. *J Cereb Blood Flow Metab* 2020; 40: 1274–1289.
13. Oliveira-Ferreira AI, Milakara D, Alam M, et al. Experimental and preliminary clinical evidence of an ischemic zone with prolonged negative DC shifts surrounded by a normally perfused tissue belt with persistent electrocorticographic depression. *J Cereb Blood Flow Metab* 2010; 30: 1504–1519.
14. Dreier JP, Fabricius M, Ayata C, et al. Recording, analysis, and interpretation of spreading depolarizations in neurointensive care: review and recommendations of the COSBID research group. *J Cereb Blood Flow Metab* 2017; 37: 1595–1625.
15. Labar DR, Fisch BJ, Pedley TA, et al. Quantitative EEG monitoring for patients with subarachnoid hemorrhage. *Electroencephalogr Clin Neurophysiol* 1991; 78: 325–332.
16. Claassen J, Hirsch LJ, Kreiter KT, et al. Quantitative continuous EEG for detecting delayed cerebral ischemia in patients with poor-grade subarachnoid hemorrhage. *Clin Neurophysiol* 2004; 115: 2699–2710.
17. Rots ML, van Putten MJ, Hoedemaekers CW, et al. Continuous EEG monitoring for early detection of delayed cerebral ischemia in subarachnoid hemorrhage: a pilot study. *Neurocrit Care* 2016; 24: 207–216.
18. Rosenthal ES, Biswal S, Zafar SF, et al. Continuous electroencephalography predicts delayed cerebral ischemia after subarachnoid hemorrhage: a prospective study of diagnostic accuracy. *Ann Neurol* 2018; 83: 958–969.
19. Nasretdinov A, Lotfullina N, Vinokurova D, et al. Direct current coupled recordings of cortical spreading depression using silicone probes. *Front Cell Neurosci* 2017; 11: 408.
20. Nasretdinov A, Evstifeev A, Vinokurova D, et al. Full-Band EEG recordings using hybrid AC/DC-Divider filters. *eNeuro* 2021; 8: 1–10.
21. Vinokurova D, Zakharov AV, Lebedeva J, et al. Pharmacodynamics of the glutamate receptor antagonists in the rat barrel cortex. *Front Pharmacol* 2018; 9: 698.
22. Dreier JP and Reiffurth C. The stroke-migraine depolarization continuum. *Neuron* 2015; 86: 902–922.
23. Stoltenburg-Didinger G and Schwarz K. Brain lesions secondary to subarachnoid hemorrhage due to ruptured aneurysms. *Stroke and Microcirculation* 1987; 42.
24. Schatlo B, Dreier JP, Glasker S, et al. Report of selective cortical infarcts in the primate clot model of vasospasm after subarachnoid hemorrhage. *Neurosurgery* 2010; 67: 721–728.
25. Fuxe K, Bjelke B, Andbjør B, et al. Endothelin-1 induced lesions of the frontoparietal cortex of the rat. A possible model of focal cortical ischemia. *Neuroreport* 1997; 8: 2623–2629.
26. Starkey ML, Bleul C, Zorner B, et al. Back seat driving: hindlimb corticospinal neurons assume forelimb control following ischaemic stroke. *Brain* 2012; 135: 3265–3281.
27. Windle V, Szymanska A, Granter-Button S, et al. An analysis of four different methods of producing focal cerebral ischemia with endothelin-1 in the rat. *Exp Neurol* 2006; 201: 324–334.
28. Wu J, Guo C, Chen S, et al. Direct 3D analyses reveal barrel-specific vascular distribution and cross-barrel branching in the mouse barrel cortex. *Cereb Cortex* 2016; 26: 23–31.
29. Dzhala V, Ben-Ari Y and Khazipov R. Seizures accelerate anoxia-induced neuronal death in the neonatal rat hippocampus. *Ann Neurol* 2000; 48: 632–640.
30. Chen S, Mohajerani MH, Xie Y, et al. Optogenetic analysis of neuronal excitability during global ischemia reveals selective deficits in sensory processing following reperfusion in mouse cortex. *J Neurosci* 2012; 32: 13510–13519.
31. Andrew RD, Hartings JA, Ayata C, et al. The critical role of spreading depolarizations in early brain injury: consensus and contention. *Neurocrit Care* 2022 doi: 10.1007/s12028-021-01431-w.
32. Fowler JC. Adenosine antagonists delay hypoxia-induced depression of neuronal activity in hippocampal brain slice. *Brain Res* 1989; 490: 378–384.
33. Katchman AN and Hershkowitz N. Adenosine antagonists prevent hypoxia-induced depression of excitatory but not inhibitory synaptic currents. *Neurosci Lett* 1993; 159: 123–126.
34. Khazipov R, Congar P and Ben-Ari Y. Hippocampal CA1 lacunosum-moleculare interneurons: comparison of effects of anoxia on excitatory and inhibitory postsynaptic currents. *J Neurophysiol* 1995; 74: 2138–2149.
35. Dzhala V, Desfreres L, Melyan Z, et al. Epileptogenic action of caffeine during anoxia in the neonatal rat hippocampus. *Ann Neurol* 1999; 46: 95–102.
36. Khazipov R, Bregestovski P and Ben-Ari Y. Hippocampal inhibitory interneurons are functionally disconnected from excitatory inputs by anoxia. *J Neurophysiol* 1993; 70: 2251–2259.
37. Somjen GG. Mechanisms of spreading depression and hypoxic spreading depression-like depolarization. *Physiol Rev* 2001; 81: 1065–1096.
38. Lipton P. Ischemic cell death in brain neurons. *Physiol Rev* 1999; 79: 1431–1568.
39. Dreier JP. The role of spreading depression, spreading depolarization and spreading ischemia in neurological disease. *Nat Med* 2011; 17: 439–447.

40. Hinzman JM, DiNapoli VA, Mahoney EJ, et al. Spreading depolarizations mediate excitotoxicity in the development of acute cortical lesions. *Exp Neurol* 2015 May; 267: 243–253.
41. Dijkhuizen RM, Beekwilder JP, van der Worp HB, et al. Correlation between tissue depolarizations and damage in focal ischemic rat brain. *Brain Res* 1999; 840: 194–205.
42. Juzekaeva E, Gainutdinov A, Mukhtarov M, et al. Reappraisal of anoxic spreading depolarization as a terminal event during oxygen-glucose deprivation in brain slices in vitro. *Sci Rep* 2020; 10: 18970.
43. Rader RK and Lanthorn TH. Experimental ischemia induces a persistent depolarization blocked by decreased calcium and NMDA antagonists. *Neurosci Lett* 1989; 99: 125–130.
44. Hartings JA, Rolli ML, Lu XC, et al. Delayed secondary phase of peri-infarct depolarizations after focal cerebral ischemia: relation to infarct growth and neuroprotection. *J Neurosci* 2003; 23: 11602–11610.
45. Nakamura H, Strong AJ, Dohmen C, et al. Spreading depolarizations cycle around and enlarge focal ischaemic brain lesions. *Brain* 2010; 133: 1994–2006.
46. von Bornstadt D, Houben T, Seidel JL, et al. Supply-demand mismatch transients in susceptible peri-infarct hot zones explain the origins of spreading injury depolarizations. *Neuron* 2015; 85: 1117–1131.
47. Hartings JA. Spreading depolarization monitoring in neurocritical care of acute brain injury. *Curr Opin Crit Care* 2017; 23: 94–102.
48. Juzekaeva E, Nasretidinov A, Gainutdinov A, et al. Preferential initiation and spread of anoxic depolarization in layer 4 of rat barrel cortex. *Front Cell Neurosci* 2017; 11: 390.
49. Basarsky TA, Duffy SN, Andrew RD, et al. Imaging spreading depression and associated intracellular calcium waves in brain slices. *J Neurosci* 1998; 18: 7189–7199.
50. Joshi I and Andrew RD. Imaging anoxic depolarization during ischemia-like conditions in the mouse hemi-brain slice. *J Neurophysiol* 2001; 85: 414–424.
51. Kaufmann D, Theriot JJ, Zyuzin J, et al. Heterogeneous incidence and propagation of spreading depolarizations. *J Cereb Blood Flow Metab* 2017; 37: 1748–1762.
52. Hossmann KA. Viability thresholds and the penumbra of focal ischemia. *Ann Neurol* 1994; 36: 557–565.
53. Fabricius M, Fuhr S, Bhatia R, et al. Cortical spreading depression and peri-infarct depolarization in acutely injured human cerebral cortex. *Brain* 2006; 129: 778–790.
54. Dreier JP, Woitzik J, Fabricius M, et al. Delayed ischaemic neurological deficits after subarachnoid haemorrhage are associated with clusters of spreading depolarizations. *Brain* 2006; 129: 3224–3237.
55. Hartings JA, York J, Carroll CP, et al. Subarachnoid blood acutely induces spreading depolarizations and early cortical infarction. *Brain* 2017; 140: 2673–2690.
56. Hartings JA and Dreier JP. Real-time detection of lesion development in acute brain injury. *J Cereb Blood Flow Metab* 2017; 37: 1550–1552.
57. Carlson AP, Shuttleworth CW, Major S, et al. Terminal spreading depolarizations causing electrocortical silencing prior to clinical brain death: case report. *J Neurosurg* 2018; 131: 1773–1779.
58. Dreier JP, Major S, Lemale CL, et al. Correlates of spreading depolarization, spreading depression, and negative ultraslow potential in epidural versus subdural electrocorticography. *Front Neurosci* 2019; 13: 373.